ADVANCED ELECTRONIC MATERIALS
www.advelectronicmat.de

Highly Sensitive Silver-Microlayer Thin Film on a pp-PFM-Modified PDMS Strain Sensor as a Versatile Tool for Stretchable Electronics Applications

*Robert Texidó, Gloria Nieva-Esteve, Joan Gilabert-Porres, Guillermo Reyes, and Salvador Borrós**

Strain sensors for wearable electronic devices have received attention due to their potential application in medicine for physiological monitoring or as part of advanced prosthetics. However, low sensitivity values as well as complex fabrication procedures remain significant challenges limiting the applicability. This work presents the fabrication of a strain sensor based on the separation of silver microplates immobilized on a stretchable substrate. The deposition of the microplates is achieved through the exposition of a glucosamine-functionalized surface to the Tollens' reagent, being a versatile fabrication methodology able to be implemented in a wide range of substrates. The obtained sensors present a high stretchability (>100%), high conductivity (10^5 S m^{-1}), good linearity ($R^2 > 0.98$ under 30% strain), good hysteresis properties, and high sensitivity (up to GF = 900 000). Hence, the sensors allow the measurement of very small deformations even in dynamic range, where it presents a stable linear response for the quantification of cyclic deformations of 0.02% strain. Moreover, the applicability of these sensors has been studied in motion-sensing devices and in a pressure sensor revealing that this technology may expand the potential applications of wearable electronic devices.

1. Introduction

Strain sensors refer to a class of electronic devices that transduce mechanical deformations into electrical signals such as voltage, resistance, and capacitance.[1] Nowadays, stretchable and wearable strain sensors represent an accurate tool to obtain physiological measurements from body stimuli with potential application in human motion detection,[2,3] care monitoring,[4,5] advanced prosthetics,[6–8] soft robotics,[9] and beyond. From a material science perspective, resistive strain sensors consist of two parts: On the one hand, the elastomeric supporting material that allows the sensor to adapt to curved and time-dependent surfaces present in the human body, such as poly(dimethylsiloxane) (PDMS),[10,11] Ecoflex[12] or Dragon Skin[13] and, on the other hand, the materials that present micro/nanostructural changes and interactions in the sensing layer that provides changes in the electrical signal during stretching. These materials are mainly metallic nanomaterials (such as nanowires[14,15] or nanoparticles[16,17]), conductive polymers (such as polypyrrole,[18,19] polyaniline[20,21] or poly(3,4-ethylenedioxythiophene) polystyrene sulfonate[22,23]) or carbon-based materials,[24,25] among others. The intrinsic union of these materials with the elastomeric matrix defines the strain-response mechanism which plays a critical role in the performance metrics of the sensors. For practical implementation, strain sensors must conform to complex biological surfaces sustaining large deformations (<50%) and presenting high sensitivity (high gauge factor GF), high stability to dynamic forces as well as high versatility to be able to fabricate complex geometries and designs,[26,27] being critical for its applicability. For the precise monitoring of diverse human activities, it is required both high stretchability and high sensitivity. Therefore, the sensor provides a stable electric signal over the entire range of strain being able to detect subtle pulse physiological signals (<5% strain) and large-scale joint motions (>80% strain). However, a sensor with high stretchability and high sensitivity is still a huge challenge because high stretchability requires an integrated structure of conductive elements maintaining an efficient charge transport at high amount of strain, while high sensitivity requires structural changes of the conductive material under very small deformations.[28] Considering all the above, high stretchable strain sensors designed for biological environments usually show low sensitivities

R. Texidó, G. Nieva-Esteve, S. Borrós
Grup d'Enginyeria de Materials (GEMAT)
Institut Químic de Sarrià (IQS)
Universitat Ramón Llull
Barcelona 08017, Spain
E-mail: salvador.borros@iqs.url.edu

J. Gilabert-Porres
Tractivus SL
Barcelona 08017, Spain

G. Reyes
Grupo de Ingeniería de Producto Industrial (GEPI)
Universitat Ramón Llull
Barcelona 08017, Spain

The ORCID identification number(s) for the author(s) of this article can be found under https://doi.org/10.1002/aelm.202200717.

DOI: 10.1002/aelm.202200717

($GF \leq 10^3$),[29,30] while highly sensitive strain sensors do not stand high amount of deformation (≤50% strain).[31,32] The challenge becomes more complicated when other required properties are considered such as performance under dynamic conditions or linearity of the output signal.[33,34] The sensor must present a clear, stable signal with a short response time in order to adapt to the sudden changes present in biological sensors. Also, nonlinear signals will be more complex to interpret and therefore more difficult to implement in a real environment.

Herein, we present an approach to solve this problem of strain sensors through a balance between their performance requirements. We present a strain sensor based on the immobilization of metallic silver microplates on PDMS modified with a polymeric thin film with metallic reduction properties. This system has been widely studied in our group as silver reservoirs to provide bacteriophobic/antibacterial properties to elastomeric materials.[35,36] However, under specific conditions of Tollens' reaction, silver nucleation produces a homogeneous surface of silver microplates that can be easily separated under stress, revealing a polymer-silver interface directly attached to the substrate that allows the electrical conductivity under high strain levels (near 100% strain). These structural changes produce variations in conductivity that, with the appropriate design, allow it to work as a highly sensitive strain sensor, reaching GF values up to 900 000. The intrinsic rigidity of the silver micro plate's structure is very low, which combined with the flexibility of the PDMS substrate can be easily adapted on the skin surface and receive large deformations without affecting the sensors' sensitivity (>100% strain). For its application in biological environments or in human motion monitoring, the sensor allows the measurement of very small deformations even in dynamic range, where it presents a stable linear response for the quantification of cyclic deformations of 0.02% strain, a stable average degree of hysteresis and a stable signal with good linearity ($R^2 > 0.98$) for deformation below 30% of strain. We have studied the ability of the presented sensors to be implemented on human monitoring devices and soft actuators, finding that the sensor is able to detect, measure and differentiate small deformations on the skin in a real environment. This, together with the intrinsic versatility of the fabrication method reflects that the presented technology is versatile, adaptable, and may lead to the obtention of new stretchable electronic devices.

2. Results and Discussion

2.1. Fabrication of Silver Microlayers on pp-PFM Modified PDMS Substrate

Figure 1a schematically illustrates the fabrication process of the plasma polymerized perfluorophenyl methacrylate (pp-PFM)/silver coating on PDMS substrate. First, a thin film of pp-PFM was immobilized on PDMS substrate through plasma polymerization of PFM acrylic monomer. This film presents high reactivity for the amino group due to the presence of the active fluorinated ester groups that promote the nucleophilic attack. In this case, pp-PFM films were exposed to glucosamine, reacting with the fluorophenyl groups and being covalently bonded to the pp-PFM chains, obtaining a sugar-functionalized surface. This functionalization allows the reduction of silver ions through Tollens' reaction as we previously reported.[36] The resultant silver coating onto the modified PDMS formed a stable metallic layer adhered to the elastomeric substrate (thickness ≈1 μm). Samples do not reveal film delamination or a generalized/local film detachment from the PDMS substrate, adapting perfectly to the deformation (Figure 1b.1) after applying different cycles of strain and deformation. The films revealed a basal electrical conductivity of 10^5 S m^{-1} indicating that the films could be implemented in electronic devices. The electrical conductivity is in agreement with the values observed in other silver-based composites where the conductivity value of bulk metallic silver has been retained.[37,38]

Field-emission scanning electronic microscopy (FE-SEM) images of the silver pp-PFM modified PDMS (Figure 1b.2, c.1,c.2) reveal that surface morphology is composed of rectangular layers of silver (length ≈100 μm). These silver layers are in contact with each other forming a continuous path that easily allows the electron mobility obtaining conductivity values closer to bulk metallic silver. A maximization of the FE-SEM microscopy image of the silver layer (Figure 1c.2) shows that these structures are conformed by silver nanoparticles (≈100 nm) unified by a coalescence phenomenon during the Tollens' reaction. This can be observed during the exposition of pp-PFM modified PDMS to silver reduction reaction (Figure 1b.2) where the characteristic "worm structure" of pp-PFM on PDMS is gradually covered by silver nanoparticles. At a specific time-point (30 min of incubation) the conductivity of the film increased from 10^2 S m^{-1} (insulator behavior) to 10^5 S m^{-1} (conductive behavior) indicating the interlocking of the formed silver microlayers that allows the electron conductivity. It is interesting to note that, when a mechanical deformation is applied to the silver samples, significative changes in the electrical conductivity are observed, returning to non-conductive values of 10^2 S m^{-1} when the samples are completely stretched before breaking. This difference of more than 8 orders of magnitude in electrical conductivity when the samples are deformed is attributed to the separation of the immobilized silver layers during the mechanical deformation (Figure 1c.1,c.2), increasing the tortuosity of the electronic pathway. Higher deformations that allow the complete separation of the silver layers show an electric resistance of 10^2 S m^{-1} that matches with the PDMS electrical conductivity. Changes in electrical conductivity present a high sensitivity during deformation, revealing a promising behavior of this coating as a strain sensor.

This strain sensor behavior of the coating has been studied through the FE-SEM microscopy at different strain rates (**Figure 2** a). At 0% of strain, the surface morphology reveals the micrometric size silver plates in contact with each other allowing the electrical conductivity (Figure 2b.1,b.2). It can be observed that defined boundaries limiting the region originated from the nucleation of metallic silver. At 20% of strain, the silver plates begin to separate revealing the connective coating between plates: a deeper region of metallic silver directly bound to the pp-PFM/glucosamine layer (Figure 2c.1,c.2). EDX analysis confirmed that this deeper region is also composed mainly by metallic silver. During the obtention of microscopy images, for samples under 20% of deformation, no specific increases in image brightness were observed that could indicate electron accumulation due to a reduction in the conductivity of the sample. This fact indicates that the interface between the substrate and the silver microplates, in addition to keeping in contact with the metallic regions, has a certain degree of electrical

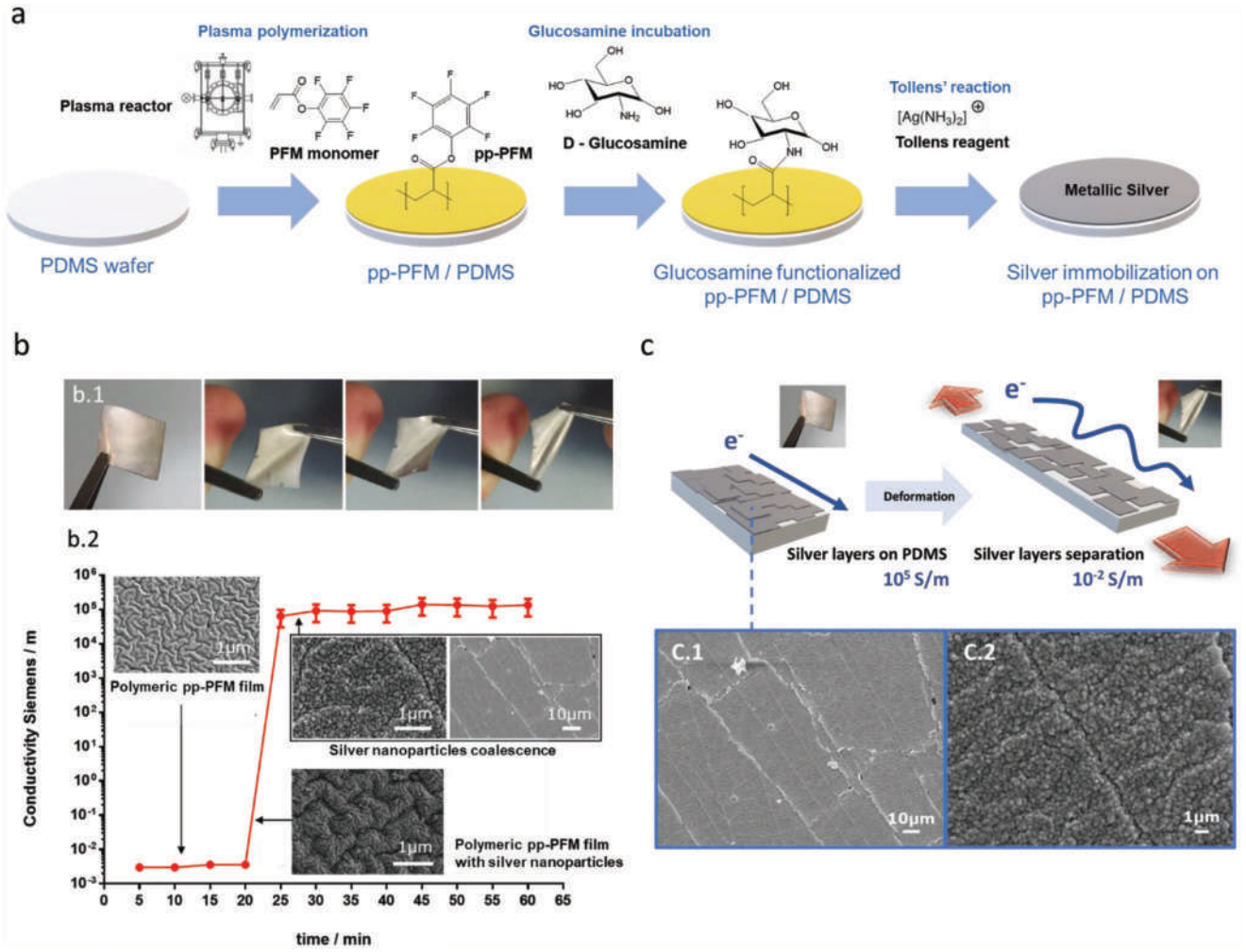

Figure 1. a) Schematics of the fabrication process of metallic silver immobilized on a PDMS substrate through the deposition of pp-PFM thin film. b.1) Images of modified pp-PFM PDMS samples after Tollens' reagent incubation. The samples present a metallic appearance even during an intensive stretch. b.2) Variation of surface conductivity depending on the Tollens' reagent incubation. The SEM images show silver morphology evolution along incubation time. c) FE-SEM image of the silver layers immobilized on modified pp-PFM PDMS samples (c.1 and c.2) and conceptualization of the mechanism for the film conductivity changes during deformation.

conductivity that allows the stability of the electrical signal during deformation. Figure 2d.1,d.2 show the arrangement of silver microplates under 100% of strain. Due to the apparition of high-brightness regions on the interphase, it can be assumed that under this percentage of deformation the silver structures are widely separated hindering the electron mobility and therefore the electrical conductivity. When the deformation is stopped, the silver microplates return to their original position even after several stretches (Figure 2e1,e.2). After analyzing the microscopy images before, after, and during the deformation, the formation or propagation of new cracks has not been observed. Through the interaction of the described silver structures under deformation, it can be explained the differences in the sensor's sensing behavior. It was not an observed coating delamination or an increase in the interface region between silver microplates during the test that reflects the good stability of the coating.

Figure 3a describes the fabrication steps for the strain sensor based on the proposed silver layers deposited on PDMS. The methodology has been designed to obtain a continuous conductive path with geometries that allow the implementation in electronic devices of more complexity. To do this, a 3D printed mask was used on PDMS to control the regions where pp-PFM is deposited, and hence the immobilization of silver layers. The mask is placed on the surface of the PDMS sample and then, inside the plasma reactor for PFM plasma polymerization. After that, the mask is gently removed from the surface of the modified pp-PFM PDMS for the incubation in the glucosamine solution and with the Tollens' reagent. At the end of the Tollens' reaction, a continuous silver path with the geometries of the mask was obtained (the fabrication process is detailed in the Experimental Section).

The masking process allows to easily obtain a conductive silver path on stretchable PDMS with a high control on the 2D geometry using a simple and cost-effective methodology. Once the sensor is fabricated, a visual inspection of the surface shows the different regions obtained: The conductive region, exposed to pp-PFM during the plasma polymerization; the insulator region,

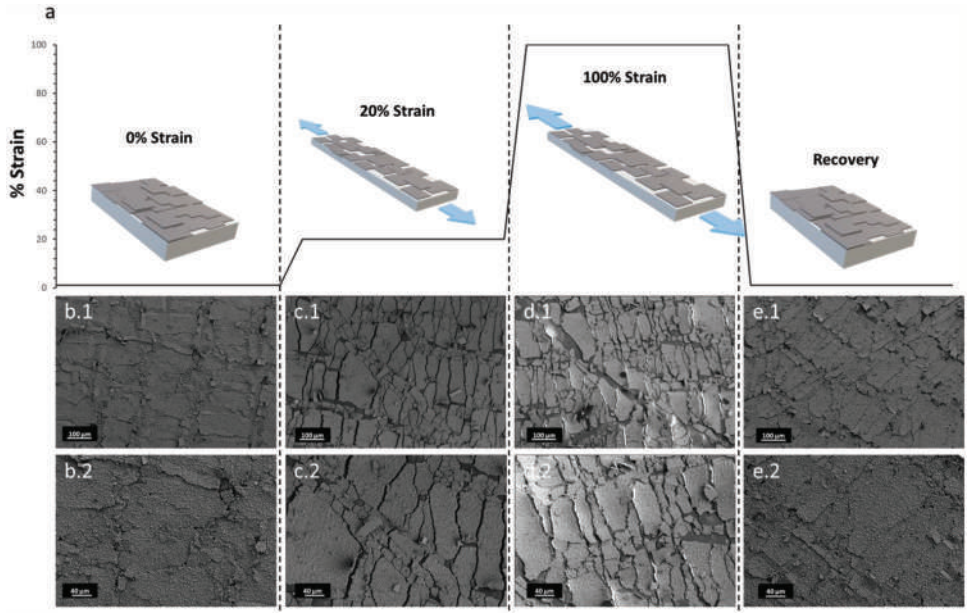

Figure 2. FE-SEM image of the silver layers immobilized on modified pp-PFM PDMS samples. a) Conceptualization of the mechanism for the film conductivity changes during deformation, b.1,b.2) silver surface at 0% of strain, c.1,c.2) silver surface at 20% of strain, d.1,d.2) silver surface at 100% of strain and e.1,e.2) silver surface after mechanical deformation.

blocked from the pp-PFM and the interphase between them. Figure 3b and its magnifications show the surface morphology of these regions revealing the silver layers with the same structure as observed in Figure 1. The regions blocked by the mask during the pp-PFM deposition show micrometric isolated clusters (≈10 µm) of silver unable to transport electrical charge. The transition between the two regions presents a smooth transition (≈100 µm) from the silver layer zone to PDMS maintaining the original geometry of the mask. The validate the versatility of the fabrication method as well as the ease in obtaining a relatively complex geometry, two sensors were evaluated in this work: a linear sensor of 20 × 1 mm and a zig-zag sensor of 25 mm length with an angle of 60° (Figure 3c.1) (specific dimensions of both sensors are detailed in Figure S1A, Supporting Information). As a qualitative test, the fabricated sensors were used as a part of an electrical set, where a voltage of 2 V allowed to light

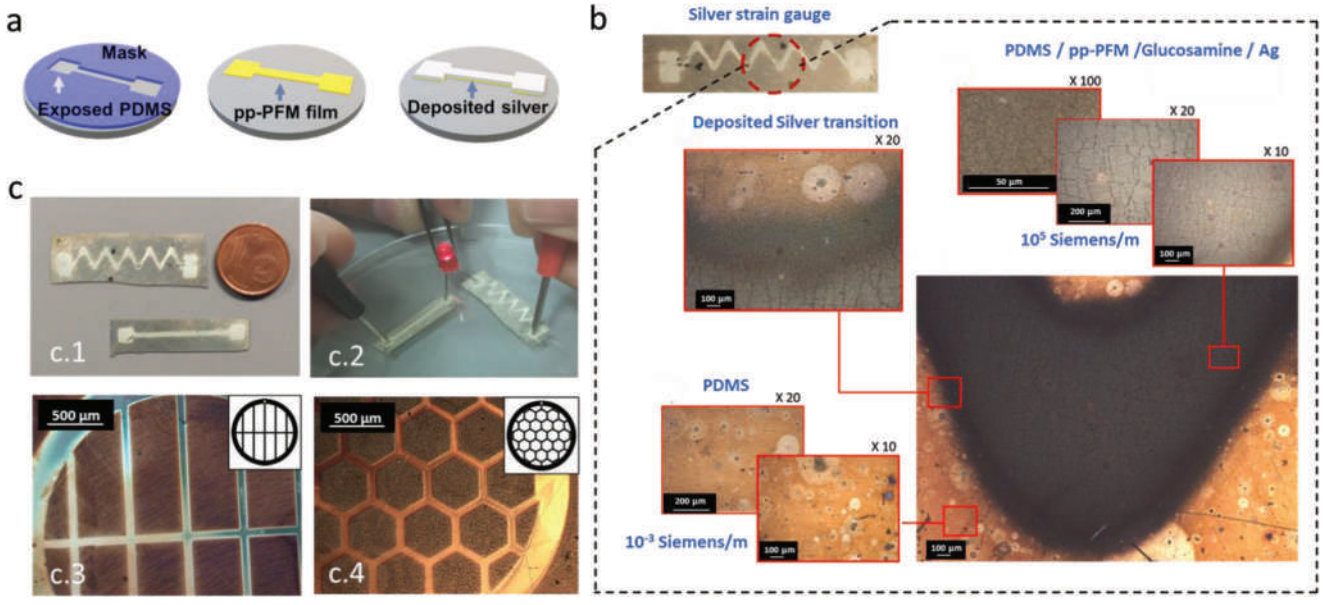

Figure 3. a) Schematics of the fabrication of strain sensor. A 3D printed mask allows the exposition of PDMS surface during plasma polymerization controlling where PFM is deposited. b) Images of the strain sensors region after the manufacturing process. c) Images of conductive silver paths created though masking fabrication process. For (c.1) and (c.2) an SEM finder grid was used as a mask while (c.3) and (c.4) show two continuous paths created with a 3D printed mask.

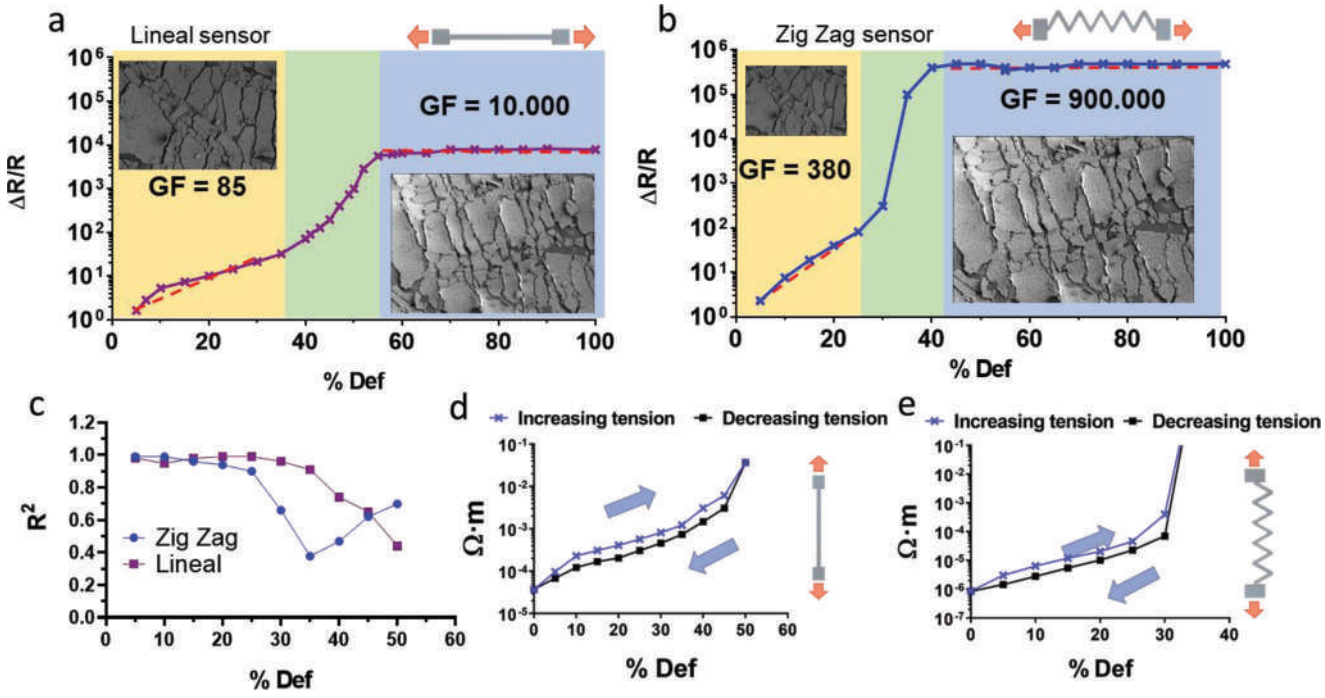

Figure 4. Evaluation of silver microlayers encapsulated on PDMS as a strain sensor. a,b) Relative resistance changes under deformation for the two evaluated designs: Linear sensor (a) and zig-zag sensor (b). c) Evolution of the sensor's linearity depending on applied deformation. d,e) Hysteresis cycles of the linear region for a linear sensor (d) and a zig-zag sensor (e).

a standard LED (Figure 3c.2). One of the most interesting features of the fabrication process consists in the obtention of conductive patterns with low values of width (below 1 mm). Main stretchable electronics fabrication technologies can easily obtain square-shaped electrodes with a wide range of length values but limited in width, where obtaining a width of less than a millimeter is a challenge.[39,40] As presented in Figure 3c.3,c.4, the fabrication method allows to recreate the geometries presented in two different micrometric cooper grids used as masks, revealing conductive regions of 420 and 430 µm respectively (measurements are detailed in Figure S1B, Supporting Information).

2.2. Silver Microlayers Encapsulated in PDMS as a Strain Sensor

To evaluate the PDMS–silver microlayers strain sensor behavior, sensors fabricated as described below were clamped on a mechanical essay machine (dynamical mechanical analysis DMA) able to provide different cyclic load conditions to the strain sensors. Simultaneously, the sensor resistivity changes were measured in real-time using the methodology and setup is described in the Experimental Section. Two strain sensors with different designs were evaluated: A conventional linear pattern was used as a reference and a zig-zag pattern to increase the sensor's active length to enhance the sensitivity. **Figure 4** shows the resistivity changes profile, while a deformation is constantly applied to the strain sensors (Figure 4a,b for the linear and zig-zag sensors respectively). The profiles revealed significant changes depending on the amount of strain applied to the sensor that produces rearrangements of the silver microplates. We identify the three regions in the graph, where the different distribution of the silver microplates can be associated to differences in the resistivity profile. In the first region (yellow), silver microplates begin to separate, revealing the secondary silver structure (interface). Since both structures present an electrical conductivity and are in contact or overlapped, the changes in resistivity are subtle in this region. At a certain value of deformation, the separation between silver microplates and silver interface increases the leading apparition of regions, where the electronic mobility is low (brightness regions in the FE-SEM images Figure 2) due to the loss of contact between the different silver structures (green region). At some point, the deformation does not affect the arrangement of silver microplates (blue region) observing that from this point; the electrical conductivity reaches a plateau. It is interesting to note that the remaining distribution maintains a certain degree of conductivity allowing the measurement of relative resistance as an output signal. The relative resistance profile observed is similar to that observed in sensors based on elastomers with conductive fillers, with the difference of this plateau stage produced by structural changes of our conductive coating.[41] This behavior allows the recovery of the position of the silver microplates and therefore reveals an improvement in the structural stability of the sensor. Although it is not possible to obtain relevant information above 60% deformation, the sensor can recover and continue to function for low deformation ranges (up to 25–30% in the studied sensors). These three regions appear in all types of samples evaluated: coated PDMS coupons, linear sensors, and zig-zag sensors. In this latter, there are slight changes in the resistivity profile due to the design of the silver tracks (Figure 4b). The tortuous geometry of the zig-zag design increases the "active direction" (direction in which the sensor receives the deformation),

increasing the transverse sensitivity.[42] Initially, at lower deformations (yellow region) both sensors presented a linear correlation between strain and relative resistance. For linear sensor, below 30% of strain, there is a linear correlation of 98%, while for the zig-zag sensor the linear correlation is 95% below 25%. The linear behavior range present in the described sensors indicates that they can be applied for the measurements of small deformations (below 30% strain) as similar to the strain sensors described in the bibliography.[43,44] As can be observed in Figure 4c, there is a loss of linearity when for deformation above 30%; however, the sensor response is still able to be measured and to provide information about the deformation through the profile changes relative resistance. We attribute this loss of linearity to the separation of the silver microplates and the apparition of the silver present in the interface. Gauge factor (GF) indicates the relative changes in electrical resistivity to mechanical strain (in this case, tension) and provides a good idea about sensors' sensitivity. Strain sensors can be used for specific applications according to their differences in the GF. Sensors with smaller GF values and larger strain ranges can be applied for the measurement of large deformations, while sensors with larger GF values and a smaller strain suit for the detection of micro deformations or vibrations. In this context, we identified the regions on the strain versus relative resistance plot where GF presents differences for the two studied sensors. Figure 4a shows the identified GF regions for the linear sensor: First, the linear zone (Def = 0 to 30%) revealed a GF value of 85. After that, the sensor's signal changes drastically when the strain is near 40%. The GF value at the beginning of the green region is ≈2000 (Def = 30 to 58%). This value provides an insight into the magnitude of the sensitivity increase; however, it lacks applicability in a real sensor. The GF for the blue region is ≈10 000 (Def > 58%). This increase in the sensitivity of the sensor is reached when the silver microplates are further apart and the space between the microplates reveals the silver interface and silicone regions with a dramatic difference in the conductivity value. Similarly, the zig-zag sensor presents a GF of 380 in the linear region (Def = 0 to 25%) and GF = 900 000 (Def > 25%). This change in the sensitivity can be explained through the changes in the design, where the silver track is more exposed to transversal deformation enhancing the "active direction" and, therefore, the sensitivity. It is important to highlight that a standard strain gauge value is comprised between 1 and 100[24,45,46] and it is considered high/ultra-high when reaches values above 100 000.[47,48] In this context, the sensors presented in this article present a GF value for a wide range of applications in the deformation range from 0 to 25%.

The hysteresis curves of the linear region of both sensors can be observed in Figure 4d,e for the linear and zig-zag sensors, respectively. The curves reveal slight differences depending on the sense of the deformation indicating the good performance of the sensor in the deformation range from 0 to 30%. These slight differences reflect the recovery of the microplates to its original position after the stress application without causing cracks or delamination.

Considering the linear behavior of both sensors, the GF values and the good hysteresis performance, the developed silver-coated zig-zag sensor shows potential as a solution to measure small changes in deformation for human motion applications. Additionally, the dynamic study of the relative resistance changes as a function of time must be performed to evaluate the suitability for this application. **Figure 5**a,b shows the relative resistance changes when a droplet of water impacts on the zig-zag sensor surface. It can be observed how the profile of relative resistance signal output reflects the exact moment of the impact of the water drop at 4.1 s of test time (Figure 5b).

The profile of relative resistance is consistent with the behavior of the water droplet on the sensor: the first sharp change at 4.1 s is attributed to the drop impact on the surface of the sensor representing a variation of 0.05 on the relative resistance. After that, there is a progressive reduction of the relative resistance attributed to the recovery of the PDMS and the extension of the water over the surface. It is interesting to note that the changes in the profile of the time-relative resistance plot (in this case, a sharp peak at 4.3 seg) provide information about the nature of the mechanical solicitation (in this case, the impact of a water droplet). To perform a quantitative analysis of the behavior of the sensor when it is exposed to very low mechanical perturbations, the linear and zig-zag sensors were placed on a dynamical mechanical equipment (Figures S2 and S3, Supporting Information).

The first test for the study of the sensor under dynamic conditions consisted in the application of a cyclic load during a long period of time (Figure 5c). The real-time changes in the relative resistance revealed that the output signal is stable during more than 3000 seg of cycling stretching at 5% (Figure 5 shows the first 250 seg). The maximization of three regions of the first 250 seg of the test shows that the sensor is able to monitor all the stretches with a regular and homogeneous shape, proving the good durability and stability of the silver sensor.

The next test was performed to determine the sensor's operational limits under dynamic conditions. To do so different cyclic loads were applied to zig-zag sensor at 1 Hz during more than 60 seg (Figure 5d). The range of strains were placed in the linear region of the sensor (0–25% strain). The strain sensing result shows that the sensor presents a higher stability for low deformations rates (0.02–5% strain), while showing a slight drift in the output signal for higher strain rates (10%). However, it can be observed that at 30% of strain this drift in the output signal has not increased significantly affecting the profile of the signal. It is interesting to note that 30% is a value of strain out of the linear region revealing a stable performance under dynamic load. The apparition of the small drift may be caused by the resonance of silicone film under cyclic load. However, the sensor signal is stable for more than 60 seg of intense signal monitoring, and its ability to detect all the stretches performed by the actuator indicating. For the study of the strain sensing under different frequencies, the test was carried out at 6% strain showing a stable output signal for the frequency ranging from 0.3 to 3 Hz (Figure 5e). We observe a similar behavior when we change the frequency, where the sensor reproduces the small deformations with high fidelity even for the 3 Hz range. The effect of the drift is clearer for the 3 Hz frequency; however, we still observed a clear profile in the sensitivity that allows us to identify each stretch performed by the actuator. It was also evaluated the sensing behavior of the sensor for small deformations (100 micrometers of clamp displacement) at slow deformation speed (10, 50, and 100 μm min^{-1}). This test revealed that

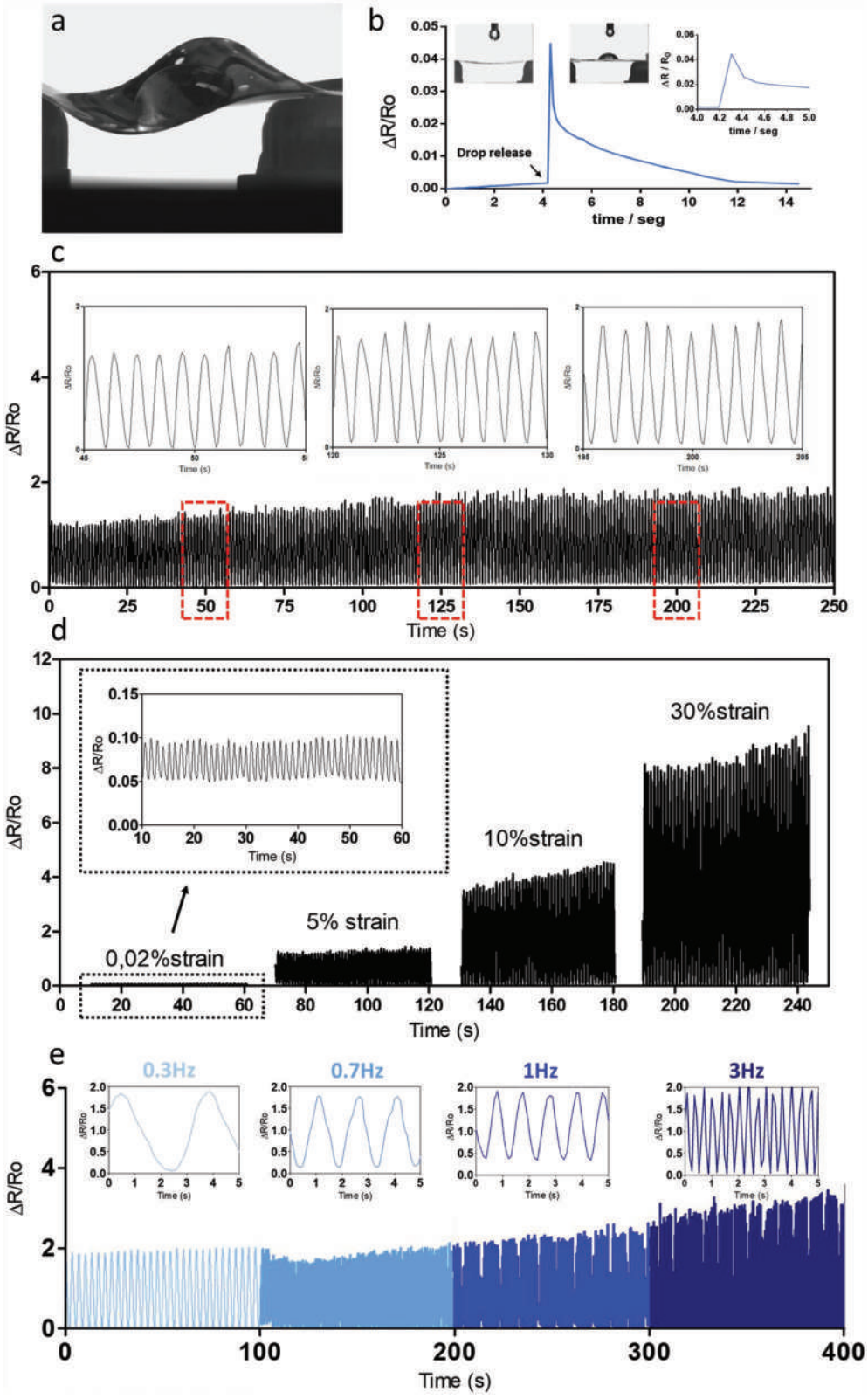

Figure 5. Characterization of minimum deformation measurable with the PDMS–silver microlayers strain sensor (zig-zag design). Sensor response to the impact of a water droplet. a) Image of the water droplet after the measurement and b) relative resistance output signal as a function of time during the impact of the water droplet (the inset shows a plot maximization on the impact point). c) Relative resistance changes at the application of cyclic micro-deformations on the linear and d–f) zig-zag sensor at different displacement/time ratios.

the relative resistance profile follows the profile of the applied deformation with a significant amount of noise (Figure S5a–d, Supporting Information). This noise is due to the vibration of the silicone substrate of the sensor being deformed at such a low speed, reflecting again the sensing ability of the sensor to detect such small deformations.

2.3. Applications and Proof of Concept

Considering the suitability of the sensors to detect small deformations, in this section two main multi-dimensional sensing applications were evaluated using the zig-zag sensor: As a human motion sensor, specifically as a kinetic sensor (for the detection of hand movements), and as a haptic button (pressure sensor), being part of a more complex device. The hand movement detection experiment was carried out by attaching the sensor on the surface of the hand to observe the correlation between the real-time hand motions and the changes in the profile of relative resistance (**Figure 6**a). The main idea is to validate if the movement of the metacarpals joint can be characterized using a PDMS–silver microlayers strain sensor. After performing a set of movements with the hand, the profile of relative resistance changed significantly as shown in Figure 6a. The profile can be divided into four regions depending on the nature of the performed movement which will be analyzed in detail below. The first section (Figure 6b) shows the output signal obtained when the hand is gently opened, placing the fingers parallel to the back of the hand, and aligned with the wrist forming a plane as can be seen in Figure 6b. This position is maintained during less than a second, returning the fingers to its starting position.

During these set of movements, the output signal reveals a sharp peak at 31.5 s corresponding with the start of the movement. The highest value of the relative resistance peak is associated with the end of the movement of the fingers while the hand is open. When the fingers begin to retract the profile of the output signal slowly decreases until it regains its original value (before the movement of the hand). Figure 6c shows a similar movement with a slight difference: after the hand was fully opened, the position of the fingers was maintained during 12 s before returning to the starting position. During this sequence, where the hand is under tension, the output signal value remained constant, while the hand was maintained open. Small peaks that appeared in these regions were attributed to micro-vibrations (tremors of the hand) indicating the good sensitivity of the sensor. It is interesting to note that when the hand recovers to its initial position, the relative resistance returns to the initial value. In this whole sequence, the value of the relative resistance is higher than in the previous sequence reflecting that it is not possible to recreate the same set of movements using the same intensity (perception of applied force and speed to perform the movement). If the same movement is performed but at a lower intensity, the value of the resistance output signal is also lower, but the profile of the curve is maintained, indicating that there are differences in the output signal that allow a reproducible identification of the metacarpal joint movements. (Figure 6d). The last set of movements presented in Figure 6e shows the changes in the output signal profile when two open-close set of movements were overlapped. As shown in Figure 6e, after the hand was fully opened, the movement of the fingers was maintained for 35 s observing a region where the relative resistance value remains constant (previously observed in Figure 6c). In this position, if the hand comes back to a fully opened position the same characteristic output signal profile was observed, revealing a sharp peak that indicates the exact moment where the hand reached the end of the opening movement. In this sense, the output signal reveals that each movement and position of the hand and fingers in the metacarpal joint can be associated with changes in the value of the relative resistance, validating the application of the PDMS–silver microlayers as strain sensors to track human motion.

The second application proof of concept was a haptic button-pressure sensor. The main idea for the construction of the sensor consisted in the attachment of two PDMS samples modified with silver microlayers in contact. The circuit setup is performed as described in the schematics of Figure 6 following the movement of the electrical charge through the silver layers. The pressure applied to the sensor reduces the distance between the silver layer enhancing the interaction between both surfaces and producing changes in the relative resistance profile. Similar to strain sensors shown before, the haptic button-pressure sensor was fabricated using the procedure based on pp-PFM PDMS modification with the masking process (Figure 6g). Resulting haptic button-pressure sensor device can be observed in Figure 6h. The changes of the relative resistance during pressure stimuli are shown in Figure 6i where the sensor was gently tapped using the index finger. The first tap was performed at $t = 13$ s, producing a sharp peak in the relative resistance profile and recovering the initial relative resistance value at $t = 16$ s. When the button-pressure sensor was kept to an intense tapping (20 taps specifically) it can be observed that the changes in the relative resistance are partly overlapped, hindering the recovery of the sensor to the initial value. However, the 20 taps performed in a narrow time-lapse (10 s) were clearly identified by a peak in the profile of the relative resistance, indicating that the sensor always produce a characteristic shape that identifies the mechanical stimuli. Both proof of concepts validate the utilization of PDMS-silver microlayers in stretchable systems to detect small stimuli for human motion sensing or as a soft pressure sensor.

3. Conclusion

We have reported a highly sensitive strain sensor fabricated by the immobilization of silver microlayers on PDMS through pp-PFM deposited by PECVD. The relationship between the arrangement of the micro silver plates and the sensor's sensing behavior has been studied finding that changes on resistivity may be correlated with the separation of the silver microplates. The obtained sensors present a high stretchability (>100%), high conductivity (10^5 S m^{-1}), good linearity ($R^2 > 0.98$ under 30% strain), good hysteresis properties and high sensitivity (up to GF = 900 000). Hence, the sensors allow the measurement of very small deformations even in dynamic range, where it presents a stable linear response for the quantification of cyclic deformations of 0.02% strain. The study of the sensor

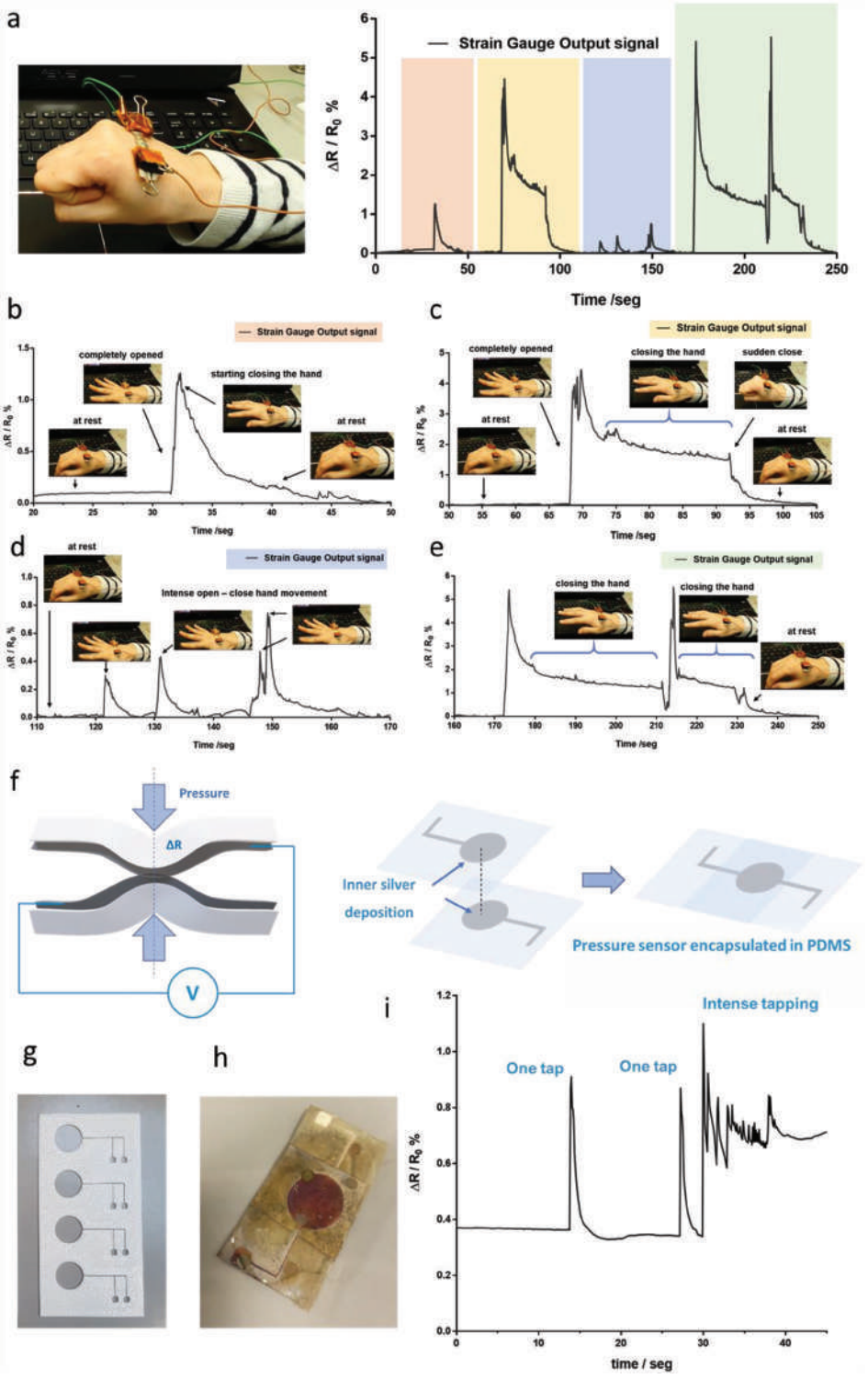

Figure 6. Hand movement detection test. a) Zig-zag sensor attached on hand surface as well as its associated output signal profile; b–e) relative resistance output signal response of zig-zag sensor under different hand movements: b) open-close hand, c) slowly close-open hand movement, d) small open-close movements, and e) continuous slow close-open hand movements. f) Design and schematics of the button pressure-sensor, g) mask used for the fabrication of the button pressure-senor, h) picture of the device, and i) output signal profile of the button pressure-sensor under tapping.

performance under dynamic conditions also revealed a clear and stable electric signal under a wide range of strains and frequencies (0–30% of strain and 0.3–3 Hz). We verified that the PDMS–silver microlayers strain sensors can be experimentally used in a variety of applications in the field of biomechanics such as human body monitoring. We performed two proofs

of concepts to evaluate the perspective of this technology to be applied on human motion sensors and soft pressure sensors. The sensors were able to detect and identify subtle deformations performed on the hand surface during a set of movements being able to correlate the profile of relative resistance with the position of the hand. For the button pressure sensor, the profile of relative resistance revealed a clear peak for each tap during a taping sequence even under an intense tapping. For both application, we observed that the main events performed on the sensors can be identified through the changes in the relative resistance profile revealing that these sensors are not only promising for stretchable electronics, but also for soft robotics and soft actuators applications and human motion sensing.

4. Experimental Section

Materials: Argon 5.0 and oxygen 5.0 were purchased from Abelló Linde S.A. (Barcelona, Spain). PFM was purchased from Apollo Scientific Ltd. (Stockport, U.K.). D-(+)-Glucosamine hydrochloride, sodium dodecyl sulfate (SDS), Hellmanex, nitric acid, and silver nitrate were purchased from Sigma-Aldrich. Ethanol was purchased from Scharlab (Barcelona, Spain), a Sylgard 184 kit was purchased from Ellsworth Adhesives (Madrid, Spain) and Si-wafers were purchased from Wafer World (West Palm Beach, FL, USA).

Substrate Preparation: The substrates used in this work were Si-wafers (as controls to validate the thickness of the silver coating) and PDMS samples (as a stretchable substrate for the fabrication of the sensor). To fabricate the PDMS plates, the Sylgard kit (10:1) was spread by a paint applicator to obtain films of 500 µm thickness. PDMS films were incubated overnight at 70 °C and after that cut in the appropriate geometry using a scalpel. It is important to denote that due to the high hydrophobicity and electrostatic charge of PDMS, samples need an accurate washing treatment. PDMS samples were washed with 5% SDS solution, rinsed with Milli-Q water, washed with 2% Hellmanex solution, and rinsed again with Milli-Q water and finally with ethanol. Si-wafers were washed with the same protocol as PDMS samples. Finally, samples were dried in a stream of nitrogen and stored.

Plasma Reactor: The surface modifications carried out in this work were performed using a stainless-steel vertical plasma reactor. This reactor consists of a stainless-steel chamber (diameter, 25.5 cm; length, 41.6 cm) vertical plate reactor (Figure S4, Supporting Information). The ground electrode was the reactor chamber, and the radio frequency (RF) electrode was an aluminum plate, which was used to hold the samples for polymerization. Additionally, the RF electrode is connected to a RF pulse generator (13.56 MHz) via a matching box. Gases and monomers were supplied via a standard manifold with gas fluxes adjusted with a tree of needle valves. The system pressure was monitored using a vacuum gauge controller (MKS PDR900, Andover, MA, USA) connected with a cold cathode/MicroPirani vacuum transducer (MKS 972 DualMag) positioned at the center of the reactor. The system had a nitrogen cold trap and a chemical trap filled with active carbon connected to avoid nonreacted monomer from reaching the pump (Trivac D 16BCS/PFPE Leybold, Cologne, Germany). The typical base pressure to all experiments was 6×10^{-4} mbar, and the monomer vapor (PFM) was introduced at a constant pressure of 0.02–0.04 mbar.

pp-PFM Thin Film Deposition: The plasma polymerization of PFM was carried out as described in the previous bibliography of our group.[49,35] Substrates were placed on an aluminum plate in the center of the reactor. Before the introduction of the substrate, the chamber was cleaned under O_2/Ar (1:1) plasma for 1 h at a power of 150 W. The continuous radio frequency power was fixed at 15 W, and pulsed plasma polymerization duty cycle (DC) of 10/20 [$DC = T_{on}/(T_{on} + T_{off})$] was carried out for 3 min. Plasma discharge was then turned off, and the PFM vapor flow was kept constant for an additional 3 min. The micropatterning/patterning process was carried out by placing the PDMS substrate on a mask with the specific geometry. As a mask for patterning, hexagonal and linear SEM copper grids (G50P, Gilder Grids, Grantham, UK) and custom 3D printed mask made of polycarbonate printed with a Stratasys Fortus 400 mc machine were used.

Silver Immobilization: pp-PFM samples were removed from the reaction chamber and incubated in a solution of glucosamine hydrochloride (1 M) at pH 7.4 during 6 h for the immobilization of the sugar. After incubation, the sugar modified PDMS surface was able to reduce silver through Tollens' method.[50] For that, samples were exposed to a concentrated Tollens' reagent during 30 min in a water bath heated at 90 °C. Tollens' reagent was prepared by adding 100 µl of sodium hydroxide (0.8 M) solution to 1 mL of silver nitrate (1 M) for silver oxidation observing a brown precipitate of silver oxide. After that, 100 µL of ammonia at 30% was added observing the complete dissolution of the precipitate indicating the complexation of silver ions by ammonia. At the end of the reaction with the Tollens' reagent, samples present an intense silver bright appearance which indicated that silver had been immobilized onto the PDMS.

Characterization: Microscopy images were obtained through field-emission scanning electronic microscopy (FE-SEM) (Zeiss Merlin). A film tension sample holder had been used to apply a specific amount of strain on the samples during the microscopy. Samples were not coated with the standard Au coating to enhance conductivity to perform the microscopy test due to its high conductivity. The thickness of the films was measured with a confocal microscope Leica DCM 3D with 50× objective (NA 0.90) obtaining an average thickness of 1 ± 0.2 µm. The modified surfaces were characterized through water contact angle (WCA; DSA100, Krüss).

Electrical Properties: The electrical properties of the strain sensors were evaluated using the same set-up previously used in our work.[51,52] Briefly, strain sensors were connected to four-point probe station (Figures S2 and S3, Supporting Information) that was connected to a source meter Keithley 2600. The sourcemeter was also connected to a PC for the obtention of the real-time data. The strain sensors were placed on mechanical test instrument (BOSE Electroforce 3200, TA Instruments) using the film tension clamps. A flexible copper band was fixed to the strain sensor using Kapton to allow electrical conductivity. This procedure ensures that the sample was not cracked before the analysis or during its set in the clamp. The inferior tension clamp was connected to a 250 N load cell which was also connected to a computer for data processing. Sample deformation and force applied to load cell were recorded in real-time. The signal output of the load cell was recorded by the measurement software WinTest from Electroforce.

The real-time resistance of the silver strain sensors was derived from amperometric *i–t* curve and the relative resistance change was determined by the equation:

$$\frac{\Delta R}{R_0} = \frac{R_r - R_0}{R_0} 100\% \tag{1}$$

where R_r represents the real-time resistance and R_0 the resistance value without an applied strain. Similarly, the *GF* was calculated as

$$GF = \frac{\frac{R_r - R_0}{R_0}}{e} \tag{2}$$

where *e* represents the applied strain.

Hand Movement Detection Tests: The volunteers who tested the devices took part in the experiments with informed consent following the assessment of any risk involved; these experiments were not subject to ethical approval.

Supporting Information

Supporting Information is available from the Wiley Online Library or from the author.

Conflict of Interest

The authors declare no conflict of interest.

Data Availability Statement

The data that support the findings of this study are available from the corresponding author upon reasonable request.

Keywords

nanostructuration, plasma polymerization, silver deposition, strain gauges, stretchable electronics

Received: June 26, 2022
Revised: October 12, 2022
Published online: November 9, 2022

[1] M. Amjadi, K. Kyung, I. Park, M. Sitti, *Adv. Funct. Mater.* **2016**, *26*, 1678.
[2] T. Yamada, Y. Hayamizu, Y. Yamamoto, Y. Yomogida, A. Izadi-Najafabadi, D. N. Futaba, K. Hata, *Nat. Nanotechnol.* **2011**, *6*, 296.
[3] C. Hou, Z. Xu, W. Qiu, R. Wu, Y. Wang, Q. Xu, X. Y. Liu, W. Guo, *Small* **2019**, *15*, 1805084.
[4] S. Xia, S. Song, F. Jia, G. Gao, *J. Mater. Chem. B* **2019**, *7*, 4638.
[5] Z. Li, Y. Wang, X. Xue, B. McCracken, K. Ward, J. Fu, *ACS Sens.* **2018**, *3*, 670.
[6] E. J. Markvicka, R. Tutika, M. D. Bartlett, C. Majidi, *Adv. Funct. Mater.* **2019**, *29*, 1900160.
[7] C. García Núñez, L. Manjakkal, R. Dahiya, *npj Flexible Electron.* **2019**, *3*, 1.
[8] G. J. Lee, C. Choi, D. H. Kim, Y. M. Song, *Adv. Funct. Mater.* **2018**, *28*, 1705202.
[9] M. Runciman, A. Darzi, G. P. Mylonas, *Soft Rob.* **2019**, *6*, 423.
[10] S. Wu, J. Zhang, R. B. Ladani, A. R. Ravindran, A. P. Mouritz, A. J. Kinloch, C. H. Wang, *ACS Appl. Mater. Interfaces* **2017**, *9*, 14207.
[11] S. Riyajuddin, S. Kumar, S. P. Gaur, A. Sud, T. Maruyama, M. E. Ali, K. Ghosh, *Nanotechnology* **2020**, *31*, 295501.
[12] M. Amjadi, Y. J. Yoon, I. Park, *Nanotechnology* **2015**, *26*, 375501.
[13] Y. Li, T. He, L. Shi, R. Wang, J. Sun, *ACS Appl. Mater. Interfaces* **2020**, *12*, 17691.
[14] D. Zhang, Z. Cheng, S. Gao, H. Shi, *Mater. Chem. Phys.* **2022**, *279*, 125730.
[15] Q. Yu, R. Ge, J. Wen, T. Du, J. Zhai, S. Liu, L. Wang, Y. Qin, *Nat. Commun.* **2022**, *13*, 778.
[16] E. Aslanidis, E. Skotadis, D. Tsoukalas, *Nanoscale* **2021**, *13*, 3263.
[17] W. Liu, Q. Chen, Y. Huang, D. Wang, L. Li, Z. Liu, *Carbon N Y* **2022**, *190*, 245.
[18] R. Texidó, S. Borrós, *Polymers* **2019**, *11*, 2108.
[19] R. Texidó, A. Orgaz, V. Ramos, S. Borrós, *Mater. Sci. Eng., C* **2017**, *76*, 295.
[20] J. Hong, Z. Pan, ZheWang, M. Y. , J. Chen, Y. Zhang, *Sens. Actuators, A* **2016**, *238*, 307.
[21] X. Xin, G. Tao, W. Biao, M. Fang, X. Dong, *Org. Electron.* **2017**, *47*, 51.
[22] M. Bhattacharjee, M. Soni, P. Escobedo, R. Dahiya, *Adv. Electron. Mater.* **2020**, *6*, 2000445.
[23] Y. Yu, S. Peng, P. Blanloeuil, S. Wu, C. H. Wang, *ACS Appl. Mater. Interfaces* **2020**, *12*, 36578.
[24] Y. Xu, X. Xie, H. Huang, Y. Wang, *J. Mater. Sci.* **2021**, *56*, 2296.
[25] Y. Yi, *J. Mater. Sci.* **2021**, *56*, 607.
[26] A. Qiu, P. Li, Z. Yang, Y. Yao, I. Lee, J. Ma, *Adv. Funct. Mater.* **2019**, *29*, 1806306.
[27] H. Souri, H. Banerjee, A. Jusu, N. Radacsi, A. A. Stokes, I. Park, M. Sitti, M. Amjadi, *Adv. Intell. Syst.* **2020**, *2*, 2000039.
[28] Z. Sun, S. Yang, P. Zhao, J. Zhang, Y. Yang, X. Ye, X. Zhao, N. Cui, Y. Tong, Y. Liu, X. Chen, Q. Tang, *ACS Appl. Mater. Interfaces* **2020**, *12*, 13287.
[29] S. Ryu, P. Lee, J. B. Chou, R. Xu, R. Zhao, A. J. Hart, S.-G. Kim, *ACS Nano* **2015**, *9*, 5929.
[30] S. Wang, P. Xiao, Y. Liang, J. Zhang, Y. Huang, S. Wu, S.-W. Kuo, T. Chen, *J. Mater. Chem. C* **2018**, *6*, 5140.
[31] J. Zhou, H. Yu, X. Xu, F. Han, G. Lubineau, *ACS Appl. Mater. Interfaces* **2017**, *9*, 4835.
[32] Y.-F. Yang, L.-Q. Tao, Y. Pang, H. Tian, Z.-Y. Ju, X.-M. Wu, Y. Yang, T.-L. Ren, *Nanoscale* **2018**, *10*, 11524.
[33] J. Jia, J. H. Pu, J. H. Liu, X. Zhao, K. Ke, R. Y. Bao, Z. Y. Liu, M. B. Yang, W. Yang, *Mater. Horiz.* **2020**, *7*, 2450.
[34] J. Jia, J.-H. Liu, S. Wang, X.-J. Zha, K. Ke, Z.-Y. Liu, P. Pötschke, M.-B. Yang, W. Yang, *Chem. Eng. J.* **2022**, *431*, 133488.
[35] C. García-Bonillo, R. Texidó, J. Gilabert-Porres, S. Borrós, *Heliyon* **2022**, *8*, e10842.
[36] J. Gilabert-Porres, S. Martí, L. Calatayud, V. Ramos, A. Rosell, S. Borrós, *ACS Appl. Mater. Interfaces* **2016**, *8*, 64.
[37] L. L. Song Chen, Y. Wei, X. Yuan, Y. lin, *J. Mater. Chem. C* **2016**, *4*, 4304.
[38] F. Xu, Y. Zhu, *Adv. Mater.* **2012**, *24*, 5117.
[39] H. Wei, K. Li, W. G. Liu, H. Meng, P. X. Zhang, C. Y. Yan, *Adv. Eng. Mater.* **2017**, *19*, 1700341.
[40] S. Yoon, H. K. Kim, *Surf. Coat. Technol.* **2020**, *384*, 125308.
[41] K. Ke, Z. Sang, I. Manas-Zloczower, *Nanoscale Adv* **2019**, *1*, 2337.
[42] J. Knapp, E. Altmann, J. Niemann, K.-D. Werner, *Measurement* **1998**, *24*, 87.
[43] X. Li, K. H. Koh, M. Farhan, K. W. C. Lai, *Nanoscale* **2020**, *12*, 4110.
[44] A. K. Bose, X. Zhang, D. Maddipatla, S. Masihi, M. Panahi, B. B. Narakathu, B. J. Bazuin, J. D. Williams, M. F. Mitchell, M. Z. Atashbar, *IEEE Sens. J.* **2020**, *20*, 12652.
[45] D. Jiang, Y. Wang, B. Li, C. Sun, Z. Wu, H. Yan, L. Xing, *Macromol. Mater. Eng.* **2019**, *304*, 1900074.
[46] M. S. Kumar, S. N. Shanmugam, *Mater. Res. Express* **2019**, *12*, 125323.
[47] Z. Liu, D. Qi, P. Guo, Y. Liu, B. Zhu, H. Yang, Y. Liu, B. Li, C. Zhang, J. Yu, B. Liedberg, X. Chen, *Adv. Mater.* **2015**, *27*, 6230.
[48] H. Li, J. Zhang, J. Chen, Z. Luo, J. Zhang, Y. Alhandarish, Q. Liu, W. Tang, L. Wang, *Sci. Rep.* **2020**, *10*, 4639.
[49] M. Artigues, J. Gilabert-Porres, R. Texidó, S. Borrós, J. Abellà, S. Colominas, *Sensors* **2021**, *21*, 4185.
[50] Y. Zhou, M. Li, B. Su, Q. Lu, *J. Mater. Chem.* **2009**, *19*, 3301.
[51] M. Zea, R. Texid, R. Villa, S. Borr, G. Gabriel, *ACS Appl. Mater. Interfaces* **2021**, *13*, 33524.
[52] R. Texidó, G. Anguera, S. Colominas, S. Borrós, D. Sánchez-García, *Polymers (Basel)* **2019**, *11*, 1068.